EPJ Photovoltaics **15**, 23 (2024)

https://doi.org/10.1051/epjpv/2024020

Available online at:
www.epj-pv.org

ORIGINAL ARTICLE OPEN ACCESS

Floating photovoltaics: modelled and experimental operating temperatures and the impact of wind speed and direction

Vilde Stueland Nysted[1,2,*], Dag Lindholm[3], Josefine Selj[1], and Torunn Kjeldstad[1]

[1] Department of Solar Power Systems, Institute for Energy Technology (IFE), 2007 Kjeller, Norway
[2] Department of Technology Systems, University of Oslo (UiO), 2007 Kjeller, Norway
[3] Department of Computational Materials Processing, Institute for Energy Technology (IFE), 2007 Kjeller, Norway

Received: 27 October 2023 / Accepted: 15 May 2024

Abstract. Floating photovoltaics (FPV) is rapidly emerging as a promising alternative to ground-mounted PV (GPV) where available land area is scarce or expensive. Improved cooling has often been reported as a benefit of FPV, as cell temperature is an important parameter for the performance of a PV system. However, more recent literature shows that the cooling effect depends strongly on FPV technology and that it is not always superior to that of open rack GPV systems. There is still a need for more information on how to estimate cell temperatures for FPV systems, and how to consider the influence of various environmental factors such as wind speed and direction. Operating cell temperature may be estimated with the PVsyst model, where heat loss coefficients (U-values) denote the heat transfer capabilities of the PV system. In this work, cell temperatures and U-values for a small footprint FPV system with east-west orientation and a 15° tilt located in Sri Lanka are studied using both module temperature measurements and computational fluid dynamics (CFD) modelling. CFD modelling allows for investigating the influence of both wind speed and direction on cell temperatures, as well as to look at the distribution of cell temperatures within the system under different wind conditions. Calculations based on measurements give $U_c = 22.6\ \mathrm{W/m^2K}$ and $U_v = 4.9\ \mathrm{Ws/m^3K}$ and correlate well with CFD calculations. We also show that wind direction, system configuration and sensor placement influence the estimated U-values, complicating the use of tabulated values for any given technology.

Keywords: Floating PV / operating temperature / cooling / U-value / CFD / wind

1 Introduction

The installed capacity of floating photovoltaics (FPV) has grown significantly in recent years, despite still being a small portion of the total PV market. As of 2021, the global installed capacity of FPV exceeded 3 GW, with the majority of installations located in Asia [1]. According to Deloitte [2], the global installed FPV capacity was expected to reach 5.2 GW by the end of 2022 and could reach 13 GW by 2025.

A main advantage of FPV over ground-mounted PV (GPV) is the reduced need for land-area, which is especially important in areas where available land is scarce and/or expensive. Additionally, there is increasing interest in combining FPV with other renewable energy sources, such as wind and hydropower, due to the potential benefits that this can offer [3–5]. Another commonly reported benefit of FPV is increased performance due to lower operating temperatures [6]. However, according to recent literature [7–9] the thermal behavior of FPV is highly technology dependent and is significantly influenced by the design of the floater structure, and whether the module is in direct thermal contact with water (water-cooled) or mounted above the water surface (air-cooled). For air-cooled systems the cooling is not necessarily better than for GPV [10–12].

The presence of the water body can affect the operating temperature of an FPV system in several ways. The air temperature is usually slightly lower above water bodies than onshore, mainly because the high heat capacity of water means it takes longer to heat up water than land [13]. Relative humidity can be higher over water than onshore [7,14], though this is not always the case [15] and the effect of higher humidity on PV operating temperatures is not clear. Some studies see increasing operating temperatures with increasing relative humidity [16,17] while some see decreasing operating temperatures with increasing relative humidity [18,19].

For FPV technologies that are not in thermal contact with water (i.e., air-cooled systems), wind is usually the most important factor for the cooling of the system, as is

* e-mail: vilde.nysted@ife.no

also the case for open rack GPV systems [20,21]. Due to the low surface roughness of water bodies, the wind speed will typically be higher over water than over land, where the presence of obstacles like vegetation and buildings will slow the wind down [22]. Given that FPV systems are typically located in windier areas than GPV systems, studying the influence of wind on module temperature is particularly important for FPV systems.

A few papers have previously reported on the dependence of operating temperatures on wind speed for FPV systems. Lindholm et al. studied the cell temperature as a function of wind speed for a Ciel et Terre system in South Africa using Computational Fluid Dynamics (CFD) modelling [23], in addition to developing a thermal model for air-cooled FPV systems [12]. A similar assessment using CFD for FPV systems has recently been published [17]. Dörenkämper et al. [8], Kamuyu et al. [24] and Tina et al. [25] all report on empirical values for heat transfer that can be applied in future energy yield assessments of other FPV systems. However, such empirical constants are both site and technology dependent, and it is therefore important with reports from a range of FPV system technologies in different climatic conditions.

Although a dependency on wind speed has been reported for FPV, there are very few reports on the impact of wind direction. A few studies on ground-mounted systems show that the wind direction also impacts the operating temperature. Two studies that report on the dependence on wind direction for the production for GPV systems in the UK both observed a greater energy production when the wind was coming from the south for south-facing systems [26,27] while Kaplani and Kaplanis (2014) reported a change in the cooling effect for varying wind incident angles [28]. Elminshawy et al. studied the influence of wind direction on the operating temperature of a partially submerged PV module using an air fan and found lowest operating temperatures when the wind came from the back and highest temperatures when the wind came from the front [29]. Chowdhury et al. studied the influence of wind direction on a single module in an FPV context using CFD modelling and found that wind direction had an impact on the operating temperature of the module, with the area of the module closest to the incoming wind being coldest [17]. However, the study does not include experimental verification of the CFD modelling and the impact of wind direction is only considered for one module, not including the floating structure.

In a previous publication, we report on the performance of the same system presented in this paper, in addition to reporting the wind-*in*dependent heat loss coefficients of the system [30]. However, the already presented work does not address the aspect of wind dependency for the heat loss coefficient. Therefore, the purpose of this work is to study the influence of wind speed and direction on the cooling of an FPV system developed by Current Solar. This has been studied through a combination of experimental measurements performed on the operating FPV system and CFD modelling. In this study, the PVsyst model is used to quantify the cooling of the FPV system. In the PVsyst model, heat loss coefficients (often referred to as *U*-values) are used as a measure of the heat transfer capabilities of the PV system [31]. Wind-dependent *U*-values have been calculated based on measured production and weather-data. Additionally, a three-dimensional CFD model of the system is used to compute operating cell temperatures of the modules and study the respective temperature variations within the system for varying wind speed and wind direction.

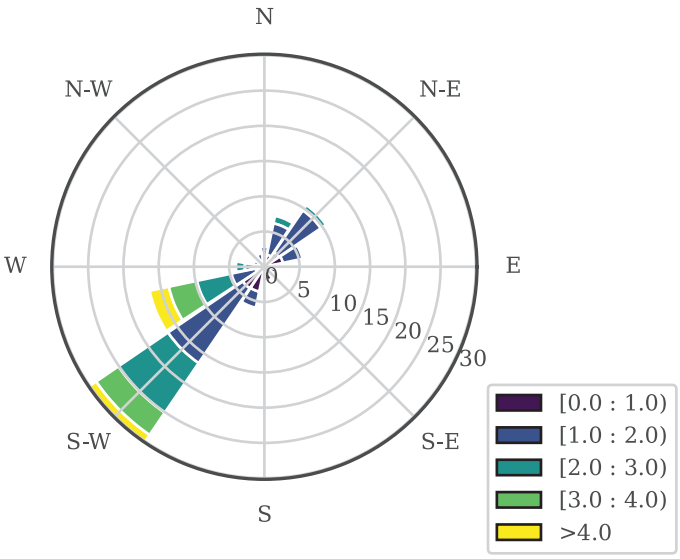

Fig. 1. Wind rose from wind measurements at the site.

2 The floating PV system in Kilinochchi, Sri Lanka

The studied FPV system is a pilot from the company Current Solar AS and has been operating since January 2020. The system has also been described in a previous publication [30]. It is installed in a freshwater body in Kilinochchi, in the province of Jaffna in Sri Lanka, at the location 9.32 N, 80.4 E. The climate at the site is characterized as a tropical rainforest, with air temperatures around 20−35 °C and high humidity all year. The hottest and most humid months are April/May and August/September, while the coolest months are December and January. From October to December, the region experiences a rainy season. The region has two main wind directions: winds are generally coming from southwest during the Southwest monsoon season from May to September and from northeast during the Northeast monsoon season from November to February [32]. The Southwest monsoon has stronger winds than the Northeast monsoon. Figure 1 shows measured wind speeds and directions at the site. The wind measurements were taken above the FPV system, at a height of approximately 1.5 m above the water, see Figure 2 for the sensor location. The measured wind directions fit well with the typical wind directions in the region, with the wind mainly coming from southwest and northeast. Wind from southeast has a spread in windspeeds from 0 to 6 m/s, while the wind from the north-east only has lower windspeeds, up to 2–3 m/s.

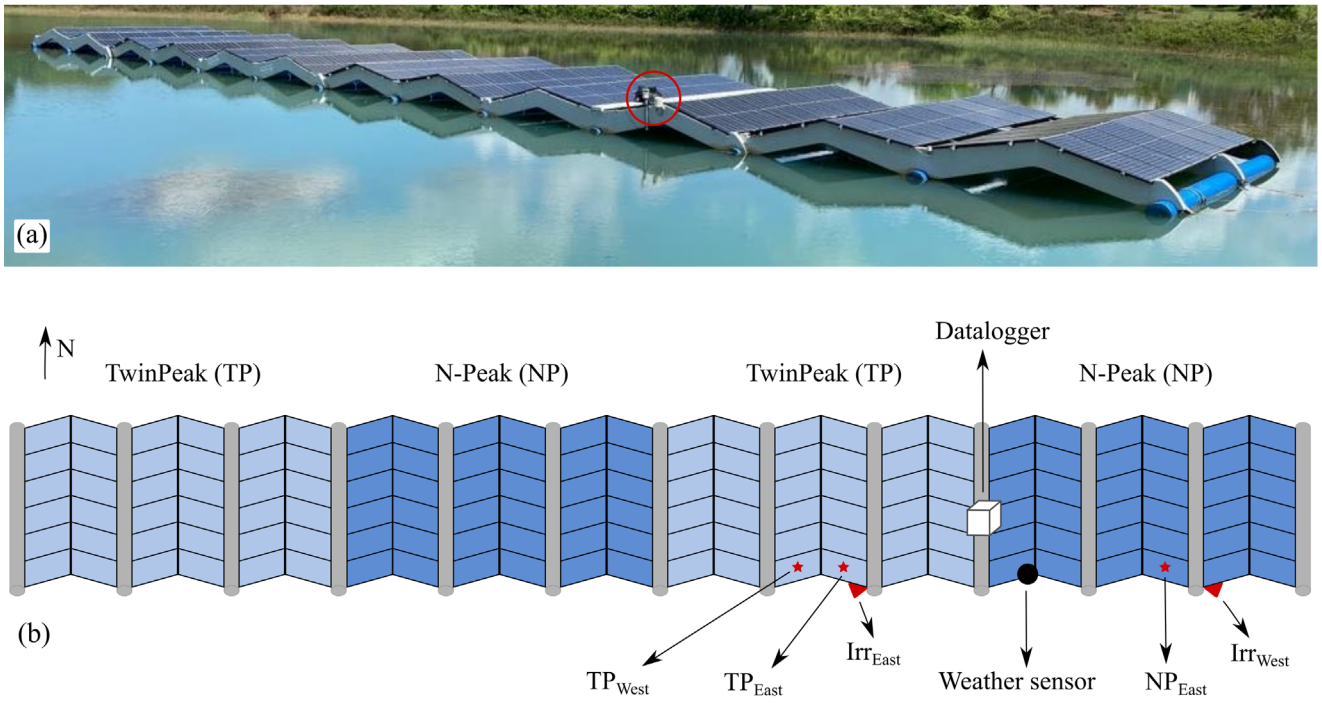

Fig. 2. (a) The FPV pilot in Kilinochchi, the ring marks the location of the weather sensor. (b) Illustration of the FPV system with the location of the different sensors. TP_{West}, TP_{East} and NP_{East} are the three back-of-module temperature sensors. Irr_{West} and Irr_{East} are the two in-plane irradiance sensors in use. The dot marks the location of the METSENS500 compact weather sensor.

The rated installed capacity of the FPV system is 44 kW. The system consists of composite beams, where the PV modules are mounted, and high-density polyethylene (HDPE) pipes that provide buoyancy to the system, as shown in Figure 2a. The PV modules are mounted vertically in an east-west orientation with a 15° tilt. Due to the anchoring design and varying water level, the system may move and change orientation to a minor degree, which leads to some uncertainty in the exact system orientation (±15°). The system has two different module types, REC Solar N-Peak 315 W (mono-crystalline n-type Si) and REC Solar TwinPeak 295 W (multi-crystalline Si). Each string is comprised of 18 modules. There are a total of eight strings in the FPV system, four with each module type. Out of the four strings for each module type, two strings are facing west and two are facing east, see Figure 2b. Each pair of strings with the same module type and orientation is connected in parallel to a separate maximum power point tracker (MPPT) on one 50 kW SMA inverter.

The FPV system fits into the "small footprint" classification suggested by Liu et al. [7], with modules mounted close to the water surface and only a smaller fraction of the underlying water covered with floats, see Figure 2a. Whilst the structure of the system is relatively open, it does to some extent limit the airflow beneath the modules.

The FPV system is instrumented with three Kipp & Zonen RT1 Smart Rooftop Monitoring Systems providing in-plane irradiance and back-of-module temperature, a Campbell Scientific 109 temperature sensor measuring water temperature, and a Campbell scientific METSENS500 compact weather sensor measuring air temperature, relative humidity, barometric pressure and wind speed and direction. The weather sensor is mounted at a height of 20 cm above the system, as can be seen in the middle of Figure 2a. Data is logged with a Campbell Scientific CR310 datalogger, with a 10-minute frequency. Figure 2b shows the placement of the sensors, where the back-of-module temperature sensors are placed in the middle of the indicated modules. For the analysis presented in this paper, all three module temperature sensors have been assessed, and referenced to as TP_{West}, TP_{East} and NP_{East}, where the abbreviations refer to the module types, REC Solar TwinPeak (TP) and REC Solar N-Peak (NP), respectively and the subscripts indicate the module orientation. In-plane irradiance has been measured using one west and one east facing sensor, shown as Irr_{West} and Irr_{East} in Figure 2b. The third RT1 irradiance sensor was defective and has not been used. In the analysis, data from September 2021 to September 2022 was used.

3 Experimental determination of *U*-value

3.1 Analytical model for *U*-values

Heat transfer between the PV module and the environment is a complex process consisting of several different physical factors. There have been numerous models proposed for simulating the operating temperature of PV systems and a review of temperature models can be found in [27]. Some of the temperature models that have been developed are quite complex, considering different factors such as convection, thermal radiation, thermal inertia, or evaporation [12,21,28–30]. Though more

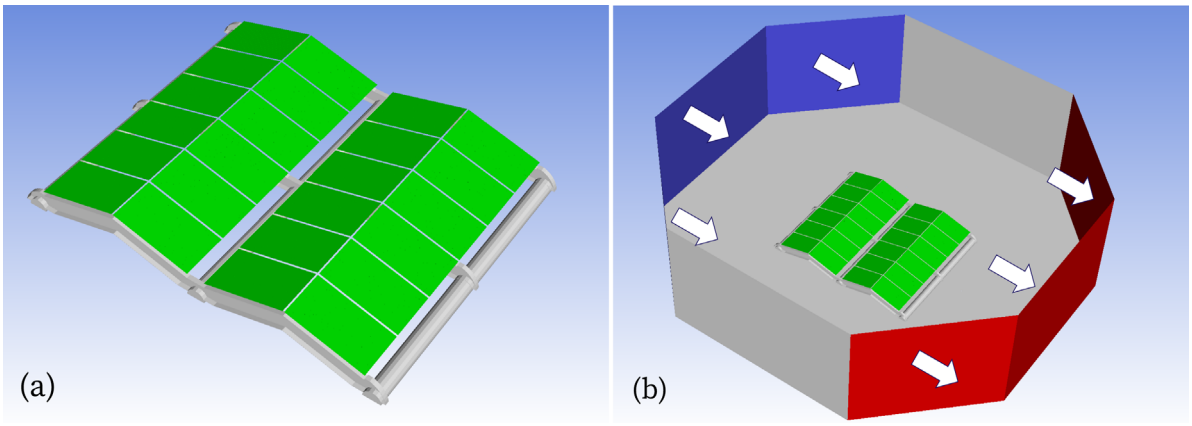

Fig. 3. (a) The model of the FPV system. (b) The computational domain.

complex models for determining module temperature exist, energy yield assessment tools often use more simplified temperature models. One of the more commonly used models is the PVsyst temperature model [31], which is based on the heat balance model by Faiman [21]. The PVsyst model is chosen in this study to simplify the use of the results towards energy yield modelling software utilized by the industry. In the PVsyst model the cell temperature, T_{cell}, is given by

$$T_{\text{cell}} = T_{\text{amb}} + \frac{\alpha \cdot G(1-\eta(T_{\text{cell}}))}{U} \tag{1}$$

where T_{amb} (°C) is the ambient temperature, G (W/m^2) is the incident irradiance, α is the absorbed fraction of the incident irradiance, $\eta(T_{\text{cell}})$ is the temperature-dependent electrical efficiency of the cell and U is the heat loss coefficient, hereby referred to as the U-value. To take the influence of wind into account, the U-value can be divided into a constant term (U_{c}) and a wind-dependent term with U_{v} as a factor: $U = U_{\text{c}} + U_{\text{v}} \times v$.

Based on equation (1), the U-value is calculated as

$$U = \frac{\alpha \cdot G(1-\eta(T_{\text{cell}}))}{T_{\text{cell}} - T_{\text{amb}}}. \tag{2}$$

Here, α is assumed to be 0.9 and a temperature corrected STC efficiency is used as $\eta(T_{\text{cell}})$. Note that in this work, the cell temperature is used to calculate the U-value instead of using the measured back-of-module temperature directly in order to compare with results from CFD modelling. The U-value is calculated separately for east facing and west facing modules, using the POA-irradiance for the corresponding direction.

Cell temperatures were estimated from the measured back-of-module temperatures using the relationship described in [33]

$$T_{\text{cell}} = T_{\text{mod}} + \frac{G}{G_0} \cdot \Delta T, \tag{3}$$

where T_{cell} (°C) is the cell temperature, T_{mod} (°C) is the back-of-module temperature, G (W/m^2) is the incident irradiance, G_0 is the reference irradiance of 1000 W/m^2 and ΔT is the temperature difference between the cell and back-of-module temperature at an irradiance of 1000 W/m^2. Here, a ΔT of 3 °C is used, as suggested for open rack modules in [33].

3.2 Data filtering

There are several factors that could influence the data quality and thus also the computed U-values, such as missing values, unphysical measurement data, stale sensor readings, sensor drift and lack of maintenance of sensors. To limit the effect of such factors on the results, the raw data was filtered before calculating U-values. Wind speed and temperature measurements outside reasonable limits were removed, as well as times with missing measurements.

Rapid changes in irradiance due to cloud movement may result in data points where the system is far from thermal equilibrium, giving incorrect estimates of the U-value. To avoid this, only periods with stable irradiance were used in the calculation of U-values. Here stable irradiance is defined as datapoints (10-minute averages) with less than 10% change in irradiance compared with the previous datapoint. In addition, only times with irradiance above 400 W/m^2 was included. When the irradiance is low the difference between ambient temperature and cell temperature can be small, meaning that small errors in measurement will have a large effect on the U-values calculated from equation (2).

4 The CFD model

4.1 The computational domain

Each module in the model of the FPV system was represented by a layer of front glass, encapsulant, wafer, and polymer back sheet. Because the size of a module is large (1675 × 997 mm) compared to its thickness (38 mm), it is a well-known challenge to make a mesh that provides sufficient accuracy at acceptable computational time. As a compromise, only 1/6th of the FPV system was included in the model. Figure 3a shows the floater structure with an assembly of 24 PV modules. To account for wind from different directions, the computational domain was constructed as an octagon, as displayed in Figure 3b.

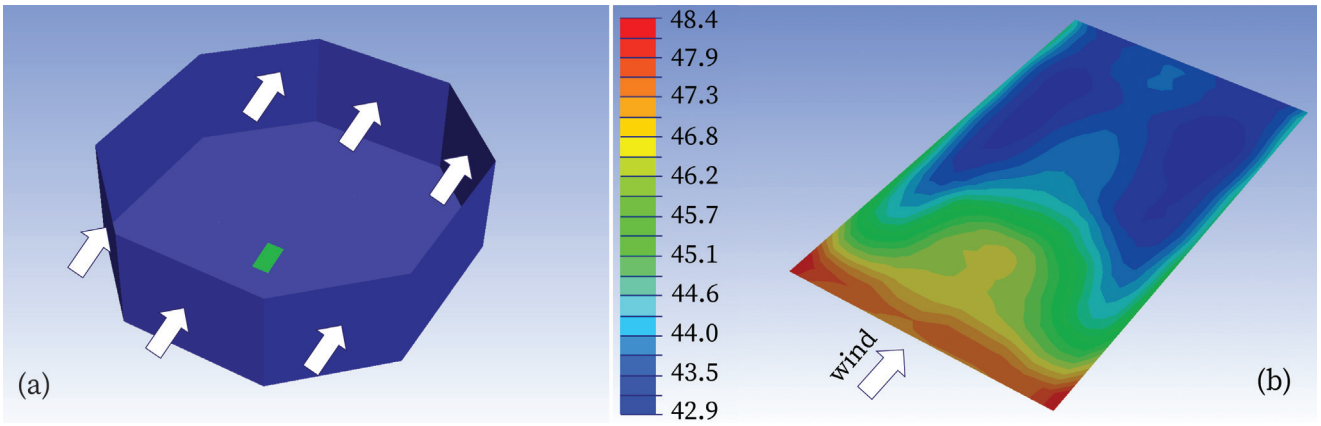

Fig. 4. (a) Model of a single, free standing PV module. (b) Computed temperatures (front glass).

Otherwise, the model setup, i.e. governing equations and boundary conditions, was equivalent to the model of a Ciel and Terre system [19], but with turbulence modelled by the k-ω model [34]. The k-ω model is considered as an all-round model good for both near-wall and free stream turbulence [35]. Since meshing the space enclosed by the back of the modules and the floater structure posed a significant challenge, the choice of turbulence model was also influenced by the fact that the equation for ω employs a y+-insensitive near-wall treatment. A flat velocity profile was imposed on the inlet with velocities ranging from 1 m/s to 5 m/s, which were typical values measured in the study. The water surface was defined as a smooth surface with zero velocity. Thermal radiation exchange with the sky and with the water body was accounted for by the Discrete Ordinates radiation model. A clear sky condition was assumed with the sky temperature modelled as [36]

$$T_{\text{sky}} = 0.0552 \cdot T_{\text{amb}}^{1.5}. \tag{4}$$

Finally, a source term that accounts for solar irradiation converted to heat in the wafer layer was added to the energy equation as

$$S_{\text{h}} = \frac{G(\alpha - \eta(T_{\text{cell}}))}{s_{\text{c}}} \tag{5}$$

where s_{c} (m) is the thickness of the cell layer, and the other terms are defined as above. ANSYS Fluent v18 was used as software.

4.2 Model verification

Even if a comparison against *U*-values derived from field measurements serves as verification of the model, a heat balance model developed by Lindholm et al. [12] and the nominal operating condition temperature (NOCT) specified by the module manufacturer was used to pre-validate the CFD model.

Figure 4a shows the model of a single PV module that is exposed to an incident solar irradiance of 800 W/m^2, a wind speed of 1 m/s, and an ambient air temperature of 20 °C, while the resulting temperatures across the front glass is shown in Figure 4b. The average cell temperature obtained in the CFD analysis was 44.5 °C, which agree well with the value computed by the heat balance model (45.5 °C) and with the temperatures specified by the module manufacturer, i.e. 44.6 ± 2 °C for REC TwinPeak 295 W and 44.0 ± 2 °C for REC N-Peak 315 W. Consequently, the uncertainty in module temperatures obtained with CFD is considered to be of the same order of magnitude as given by the module manufacturer, i.e. ± 2 °C.

5 Results

5.1 *U*-values derived from measurements

U-values were calculated according to equation (2), after filtering of the data as explained in Section 3.2. The calculations were done separately for the three module temperature sensors, NP_{East}, TP_{East} and TP_{West}. Figure 5 shows the resulting *U*-values plotted as a function of the measured wind speed. As has also been shown previously [20,21] there is a linear trend between the computed *U*-value and the wind speed. A linear fit was found using least squares linear regression, and the fitted line is included in Figure 5. Table 1 shows the calculated values of U_{c} and U_{v}, as well as the R^2 value for the linear regressions and the *t* test results for the slope (U_{v}).

5.2 *U*-values derived from modelling

All computations were based on a constant incident solar irradiance of 800 W/m^2, an ambient air temperature of 20 °C, and a water temperature of 20 °C. The temperature distribution in the cell layers was then computed for wind speeds ranging from 1 m/s to 5 m/s for 8 different wind directions. Resulting cell temperatures based on a wind speed of 3 m/s from three wind directions are displayed in Figure 6. The average cell temperature for each PV module in the system was calculated, giving minimum and maximum temperatures of 37.3 °C and 41.1°C when the wind comes from the front (Fig. 6a), 35.2 °C and 42.6 °C when the wind comes from the diagonal (Fig. 6b) and 34.7 °C and 44.6 °C when the wind comes from the side (Fig. 6c). The PV modules associated with these

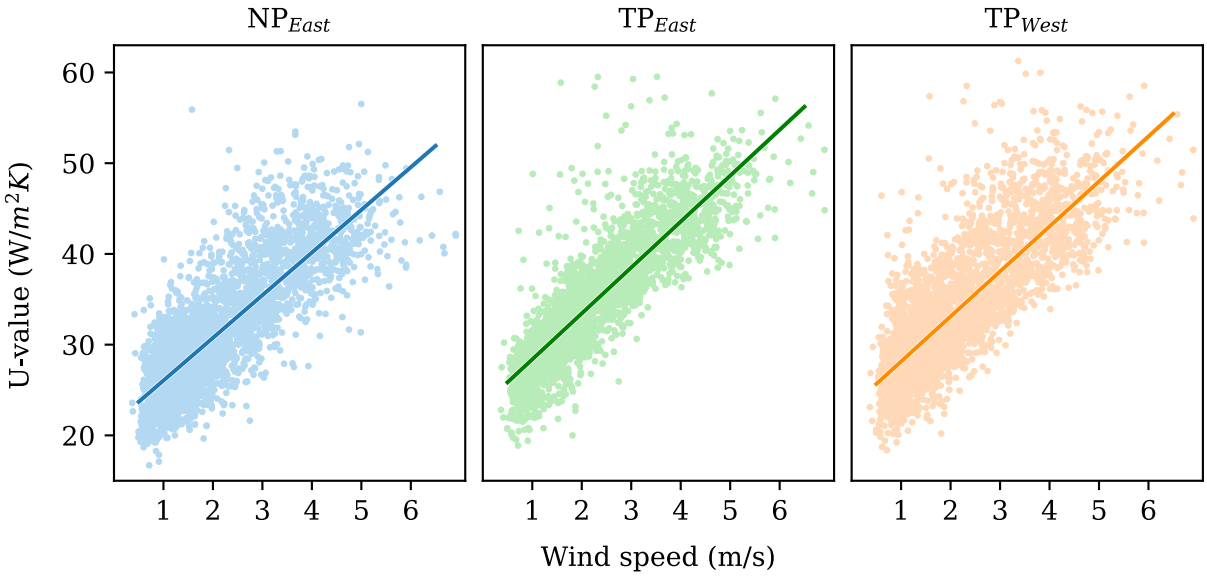

Fig. 5. *U*-values calculated from measurements for each of the three module temperature sensors plotted as a function of the wind speed. The dots show the spread in the calculated values while the solid line shows the fitted linear regression. The figure includes all data points left after performing the filtering stated in Section 3.2.

Table 1. Constant (U_c) and wind dependent (U_v) *U*-values, the R^2 value for the linear regression and the *t* test results for the slopes (U_v). The *p* value is <0.05 for all linear regressions performed. Therefore, a significant correlation between the wind speed and the *U*-values can be assumed.

	NP_{East}	TP_{East}	TP_{West}	Average
U_c [W/m^{2}K]	21.3	23.3	23.2	22.6
U_v [Ws/m^{3}K]	4.7	5.1	5.0	4.9
R^2	0.66	0.76	0.65	0.66
t test result	$t(3673) = 84.1$, $p < .001$	$t(3673) = 108.4$, $p < .001$	$t(3673) = 82.2$, $p < .001$	$t(11023) = 148.1$, $p < .001$

temperatures are marked in Figure 6. The average cell temperature for the whole system for the three wind directions is 39.4 °C when the wind comes from the front, 38.1 °C when the wind comes from the diagonal and 40.2 °C when the wind comes from the side. The computations show that the temperature distribution both across each module and across the assembly of modules is highly non-uniform and depends strongly on the wind direction and, as shown later, on the wind speed.

The cell temperature variation among the modules in the system is reflected in a similar variation in the *U*-values. The lowest temperature gives the largest *U*-value and vice versa. Based on wind directions as shown in Figure 6 and a wind speed of 3 m/s, Table 2 summarizes the maximum and minimum *U*-values obtained for the PV modules in the system, as well as the average *U*-values for the whole system. These values demonstrate well the large variation in the *U*-values across the FPV system.

For FPV systems that are mainly air-cooled, the cell temperature depends significantly on irradiance, ambient temperature, and wind speed, while the *U*-value is mainly a function of the wind speed [12,23] and, as shown below, the wind direction. Because measurement data from the site contained numerous combinations of irradiance and ambient temperature, it was convenient to convert the cell temperatures to *U*-values using equation (2) before comparing with results from measurements. Figure 2b identifies the three modules equipped with temperature sensors, TP_{West}, TP_{East} and NP_{East}. The module marked with a red dot in Figure 7a represents a monitored module. Figure 7b shows the wind-dependent *U*-values computed for the monitored module, for wind speeds ranging from 1 m/s to 5 m/s and the 8 wind directions shown in Figure 7a. The average cell temperature of the marked module was used when calculating the *U*-values. Besides confirming the linear dependency of the *U*-value on the wind speed, which is generally assumed for FPV technologies that are mainly air-cooled, the results also reveal a significant influence of the wind direction. Within the range of wind speeds that were considered, the ratio of the largest to the smallest *U*-value increases from 1.25 (at 1 m/s) to 1.51 (5 m/s). Most efficient cooling of the marked module is achieved when the wind is in direction 90°, worst when it is in direction 270°.

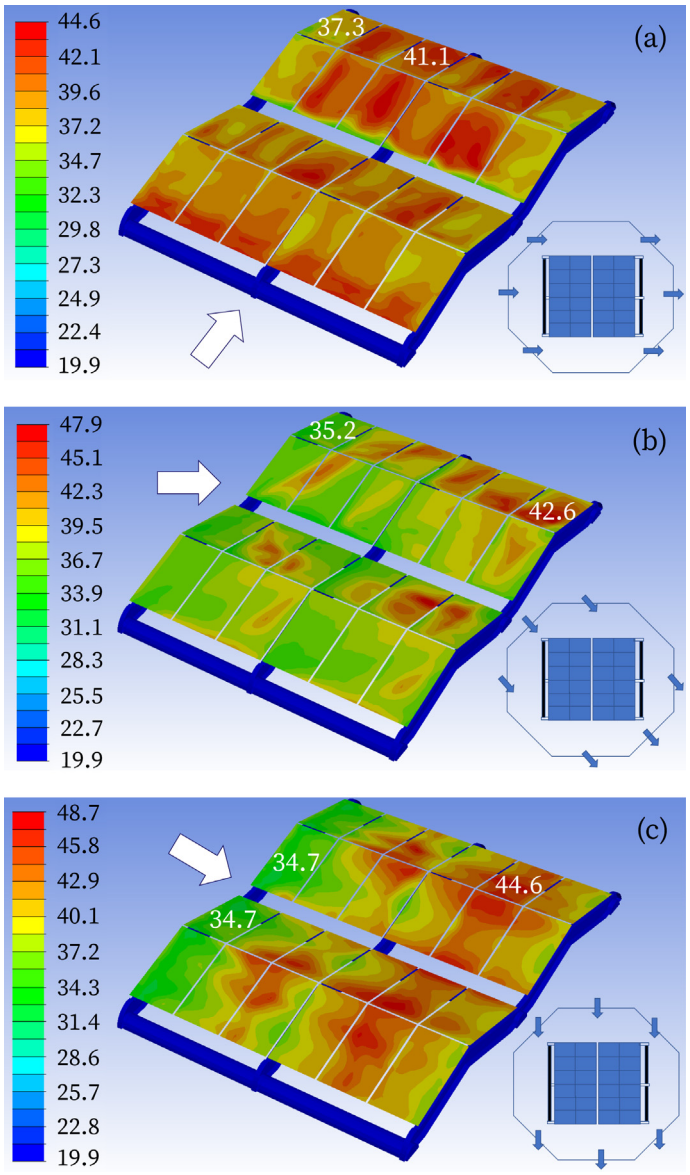

Fig. 6. Cell temperatures computed from CFD modelling based on a wind speed of 3 m/s. Average cell temperatures for each module in the system were computed and the minimum and maximum average cell temperatures are shown by white-colored values on the associated modules. (a) Wind from the front. (b) Wind from the diagonal. (c) Wind from the side.

Table 2. Maximum and minimum U-values for the PV modules in the system and average U-values for the whole system at a wind speed of 3 m/s. Values in parenthesis are the average cell temperatures used to compute the U-values.

Attack angle of wind	Maximum U-value	Average U-value	Minimum U-value
From front (Fig. 6a)	35.5 W/m^2K (37.3 °C)	31.7 W/m^2K (39.4 °C)	29.1 W/m^2K (41.1 °C)
From diagonal (Fig. 6b)	40.5 W/m^2K (35.2 °C)	34.0 W/m^2K (38.1 °C)	27.2 W/m^2K (42.6 °C)
From side (Fig. 6c)	41.8 W/m^2K (34.7 °C)	30.4 W/m^2K (40.2 °C)	25.0 W/m^2K (44.6 °C)

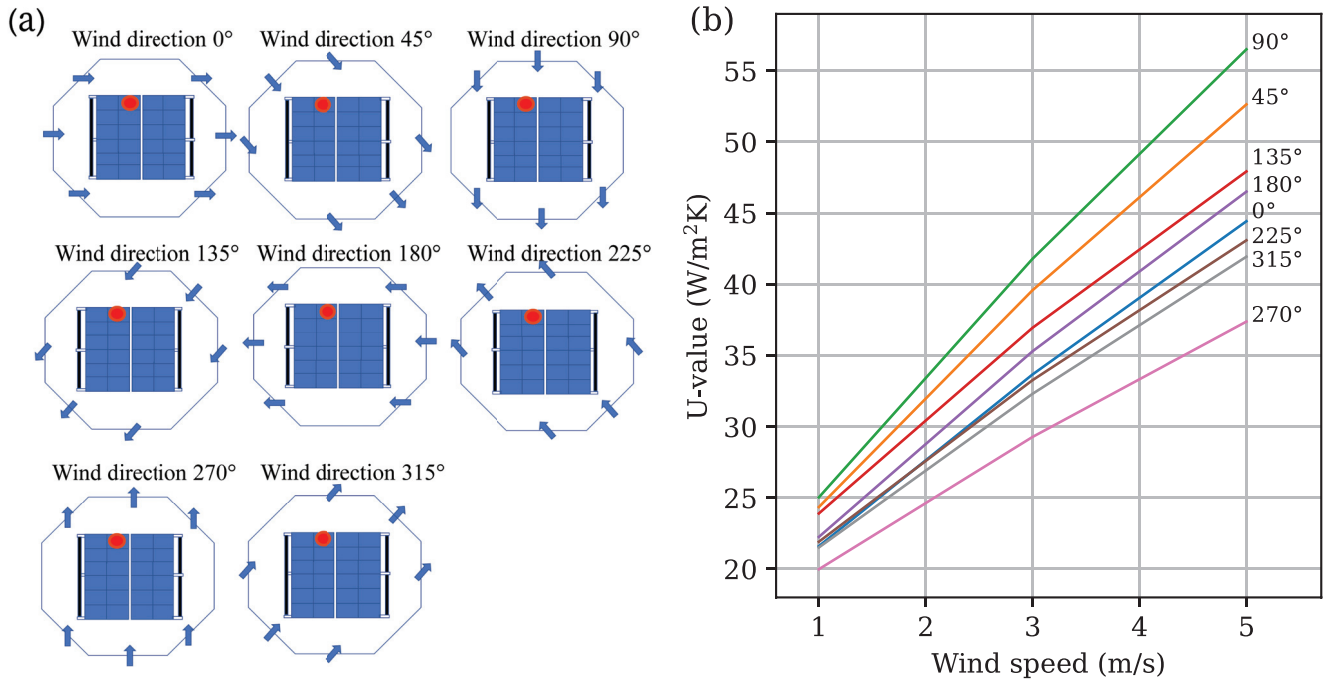

Fig. 7. (a) Wind directions and identification of a monitored module (red dot). (b) Wind-dependent U-values for the monitored module for the different wind directions.

6 Discussion

6.1 Comparison between experimentally obtained and modelled *U*-values

Due to the non-uniform cell temperature distribution across the system shown in Section 5.2, some considerations have been taken before comparing U-values derived from modelling with those derived from measurements, to ensure a fair comparison. Firstly, the U-values were modelled at locations corresponding to the placement of the back-of-module temperature sensors, see Figure 7a. Secondly, wind directions for modelled U-values were chosen to correspond with measured wind directions. According to standard IEC61853-2 [37], a range of wind speeds of at least 4 m/s is needed to calculate the wind dependent U-value. As shown in Figure 1 in Section 2, only the prevailing wind direction, southwest, has a large enough span in measured wind speeds to calculate wind dependent U-values. Therefore, only measurements recorded under these wind conditions have been included in the comparison. Wind from southwest corresponds to a modelled wind direction of 135° for temperature sensor TP_{West} and 45° for the sensors TP_{East} and NP_{East}.

Figure 8 shows the U-values obtained from measured data for south-westerly winds together with the modelled U-values for the corresponding wind directions. The curve from the modelling results has a slightly steeper slope than the measurement results, but the modelling results are within the spread of the U-values calculated from measurements and are considered to give acceptable agreement. Also considering that there is a significant variation in the temperature across each module, as seen from Figure 6, U-values derived from measurements and CFD were assessed to agree well. As indicated by the varying operation temperature within the system, see Figure 6, the wind speed will vary within the FPV system and is influenced by the floating structure and the PV modules themselves. Although this is taken into consideration in the CFD model, the wind speed variations between the weather station and module temperature sensor on site is not considered for the report on measured U-values. For the U-values computed from measurements, a constant wind speed at all points in the system equal to the wind speed measured at 1.5 m height is assumed. It is likely that the wind speed underneath the module is slightly lower than what is measured, causing an inaccuracy in the reported measured U-values.

6.2 *U*-values derived using cell temperature vs back-of-module temperature

In this study cell temperatures have been estimated based on the measured back-of-module temperatures and used in U-value calculations, instead of using the back-of-module temperatures directly, as is often done. To see how large the difference is between using estimated cell temperatures versus back-of-module temperatures, U-values for this system were calculated also using the back-of-module temperatures directly, giving an average of $U_c = 24.1\ \mathrm{W/m^2K}$ and $U_v = 6.7\ \mathrm{Ws/m^3K}$ for the three temperature sensors. Figure 9 shows the resulting U-values calculated both from cell temperatures and back-of-module temperatures. There is a prominent difference between the two, especially for higher wind speeds. This means that it is important to consider whether the U-value is based on module

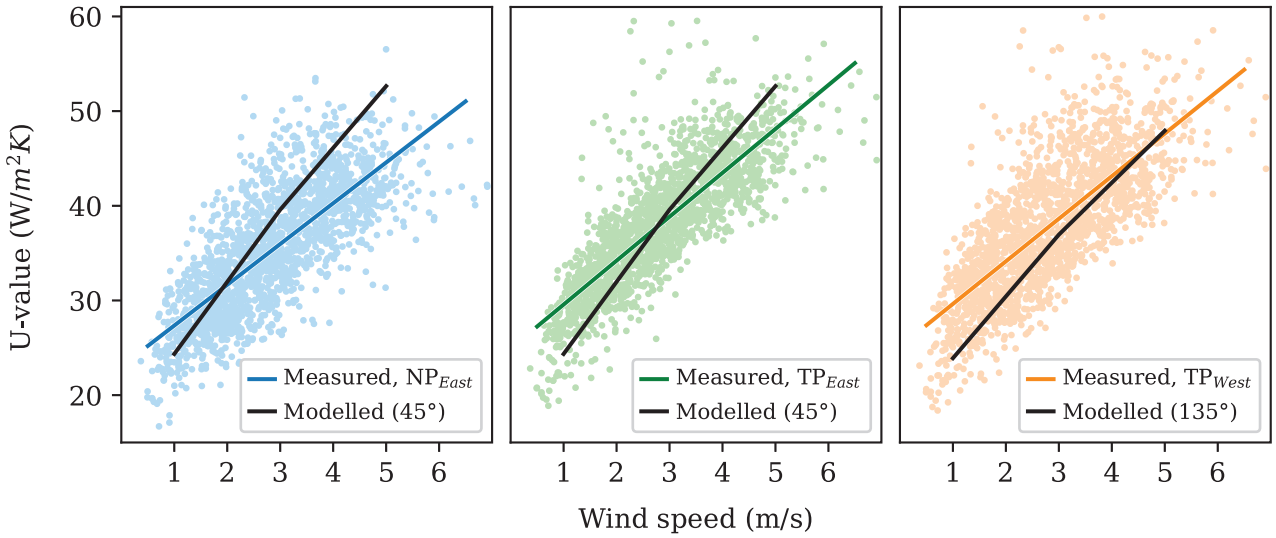

Fig. 8. A comparison between the U-values calculated from measurements and from the CFD modelling. Only measurements where the wind is coming from the southwest direction is included, and the values are compared with the modelling results from the corresponding wind direction.

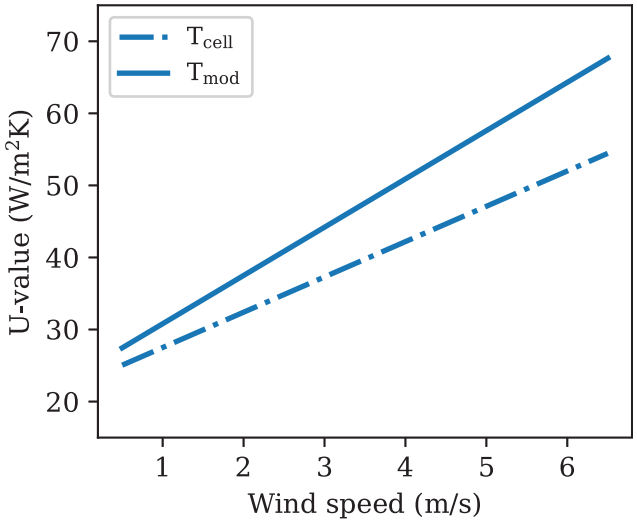

Fig. 9. U-values for the Current Solar system calculated using measured back-of-module temperatures directly (solid line) and calculated using estimated cell temperatures (dash-dotted line).

or cell temperatures when using U-values derived from experimental data to compute cell or module temperatures. As an example, the commonly used software PVsyst applies a variation of the Faiman model to compute cell temperatures [31], hence experimentally determined U-values based on cell temperatures should be used for this case.

6.3 Considerations for experimentally obtained *U*-values

Both the speed and attack angle of the wind impact the cooling of the PV modules, and hence their individual U-values. The floating structure disrupts the wind leading to an air flow over the collection of PV modules that varies locally between the different modules. As a result, a highly non-uniform temperature distribution both across each module and across the assembly of modules is seen in the modelling results in Section 5.2. In general, the module temperature is lower closer to the direction the wind is coming from and at the edges of the system. Non-uniform temperature distributions across modules and systems have also been observed in earlier literature. Goverde et al. [38] found increasing cell temperatures when moving downwind on a PV module in a wind tunnell. Faiman [21] observed varying temperatures within PV modules in a GPV system, with the center cell being warmer than the corner cell. For FPV systems, Dörenkämper et al. [8] observed higher measured module temperatures for modules more towards the center of the system compared to the outer modules.

Due to the variations in temperature across both individual modules and the whole system, a U-value determined by measurements on a single point on one module is not necessarily representative for the whole collection of modules. This is exemplified in Table 2, which illustrates the range of U-values observed for individual PV modules in the system, by showing the maximum and minimum U-values. These U-values were calculated from the average cell temperatures of the PV modules with lowest and highest average cell temperature. In Table 2, a ratio between maximum and minimum U-value of up to 1.67 is seen. This shows that care should be taken when using experimentally found U-values and the location of the temperature sensors within the system considered.

The results in Section 5.2 also show variations both in the cell temperature distribution within the system and the average cell temperature for the whole system for different wind directions. Equivalent systems with a temperature sensor placed in the same location in the system might therefore give different U-values if the systems were placed in locations with different prevailing wind directions. The prevailing wind directions at the site in relation to the location of the temperature sensors should therefore be considered when using U-values from one system in another location or when comparing systems at different locations.

7 Conclusions

In this work, wind-dependent U-values for a small footprint FPV system situated in Sri Lanka have been derived both from measurements on site throughout one year of operation and CFD modelling, with the measurements giving $U_c = 22.6\,W/m^2K$ and $U_v = 4.9\ Ws/m^3K$ and the modelling giving $U_c = 16.9\,W/m^2K$ and $U_v = 5.9\ Ws/m^3K$ (averaged for all wind directions). The CFD model was developed based on the system and verified with a heat balance model and NOCT values. The results from measurements and modelling were shown to be in good agreements when comparing similar wind direction scenarios.

In addition to the calculated U-values, the influence of both wind speed and direction on the cell temperatures, as well as the distribution of cell temperatures within the system was studied and some key findings are:

- Significant variations in operating temperature both within one single module and across the whole system were observed. This implies that measured module temperatures, and consequently also estimated U-values, depend on the location of the sensor within the system. It is therefore important to report on the placement of temperature sensors used for U-value calculations. Sensor placement should be considered when assessing how the estimated U-value represents the whole system and how applicable the U-value is for a new system.
- The wind direction will influence both the temperature distribution within the system and the average temperature of the system. Wind directions at the site should therefore be reported together with the experimentally obtained U-values and considered when using these U-values in energy yield estimations.
- The difference in U-value calculated using measured back-of-module temperatures and estimated cell temperatures underlines the importance of vigilance when applying said U-values in energy yield assessment tools.

Acknowledgments

We would like to thank Equinor and Torgeir Ulset from Current Solar for facilitating the project and sharing the production data, and Rugile Balciunaite for the photo of the system. Thanks also to Professor Dhayalan Velauthapillai and collaboration with the University of Jaffna.

Funding

This work was supported by the Norwegian Research Council through the projects FLOW (grant number 308800) and HydroSun (grant number 328640).

Conflicts of interest

The authors have nothing to disclose.

Data availability statement

Restrictions apply to the availability of these data. Data was obtained from Current Solar and are available only with the permission of Current Solar and IFE.

Author contribution statement

Vilde Stueland Nysted: Methodology, Software, Writing – Original Draft, Visualization. Dag Lindholm: Methodology, Software, Validation, Writing – Original Draft. Josefine Selj: Writing – Review & Editing, Funding acquisition. Torunn Kjeldstad: Methodology, Writing – Review & Editing, Project administration.

References

1. IEA, Trends in photovoltaic applications, 2022. www.iea-pvps.org
2. K. Ramachandran, P. Lee, M. Motyka, Floatovoltaics enters the renewable energy mix: Floating solar panels are now commercially viable, Deloitte Insights (2021). https://www.deloitte.com/global/en/our-thinking/insights/industry/technology/technology-media-and-telecom-predictions/2022/floatovoltaics-floating-solar-panels.html
3. G. Kakoulaki, R. Gonzalez Sanchez, A. Gracia Amillo, S. Szabo, M. De Felice, F. Farinosi, L. De Felice, B. Bisselink, R. Seliger, I. Kougias, A. Jaeger-Waldau, Benefits of pairing floating solar photovoltaics with hydropower reservoirs in Europe, Renew. Sustain. Energy Rev. **171**, 112989 (2023). https://doi.org/10.1016/j.rser.2022.112989
4. X. Costoya, M. deCastro, D. Carvalho, B. Arguilé-Pérez, M. Gómez-Gesteira, Combining offshore wind and solar photovoltaic energy to stabilize energy supply under climate change scenarios: a case study on the western Iberian Peninsula, Renew. Sustain. Energy Rev. **157**, 112037 (2022). https://doi.org/10.1016/j.rser.2021.112037
5. N. Lee, U. Grunwald, E. Rosenlieb, H. Mirletz, A. Aznar, R. Spencer, S. Cox, Hybrid floating solar photovoltaics-hydropower systems: benefits and global assessment of technical potential, Renew Energy **162**, 1415 (2020). https://doi.org/10.1016/j.renene.2020.08.080
6. World Bank Group, Where Sun Meets Water: Floating Solar Market Report, Washington, DC, 2019. www.worldbank.org.
7. H. Liu, V. Krishna, J. Lun Leung, T. Reindl, L. Zhao, Field experience and performance analysis of floating PV technologies in the tropics, Prog. Photovolt.: Res. Appl. **26**, 957 (2018). https://doi.org/10.1002/pip.3039
8. M. Dörenkämper, A. Wahed, A. Kumar, M. de Jong, J. Kroon, T. Reindl, The cooling effect of floating PV in two different climate zones: a comparison of field test data from the Netherlands and Singapore, Solar Energy **214**, 239 (2021). https://doi.org/10.1016/j.solener.2020.11.029
9. T. Kjeldstad, D. Lindholm, E. Marstein, J. Selj, Cooling of floating photovoltaics and the importance of water temperature, Solar Energy **218**, 544 (2021). https://doi.org/10.1016/j.solener.2021.03.022
10. L. Micheli, The temperature of floating photovoltaics: case studies, models and recent findings, Solar Energy **242**, 234 (2022). https://doi.org/10.1016/j.solener.2022.06.039

11. I.M. Peters, A.M. Nobre, Deciphering the thermal behavior of floating photovoltaic installations, Solar Energy Adv. **2**, 100007 (2022). https://doi.org/10.1016/j.seja.2021.100007
12. D. Lindholm, T. Kjeldstad, J. Selj, E.S. Marstein, H.G. Fjær, Heat loss coefficients computed for floating PV modules, Prog. Photovolt.: Res. Appl. **29**, 1262 (2021). https://doi.org/10.1002/PIP.3451
13. L. Liu, Q. Wang, H. Lin, H. Li, Q. Sun, R. Wennersten, Power generation efficiency and prospects of floating photovoltaic systems, Energy Procedia **105**, 1136 (2017). https://doi.org/10.1016/j.egypro.2017.03.483
14. S.Z. Golroodbari, W. van Sark, Simulation of performance differences between offshore and land-based photovoltaic systems, Prog. Photovolt.: Res. Appl. **28**, 873 (2020). https://doi.org/10.1002/pip.3276
15. B. Amiot, M. Chiodetti, R. Le Berre, K. Radouane, D. Boublil, P. Dupeyrat, K. Vermeyen, S. Giroux-Julien, Floating photovoltaics – on-site measurements in temperate climate and lake influence on module behavior, in *37th European Photovoltaic Solar Energy Conference and Exhibition* (2020), pp. 1772–1776
16. J. ho Choi, J.H. Hyun, W. Lee, B.G. Bhang, Y.K. Min, H.K. Ahn, Power performance of high density photovoltaic module using energy balance model under high humidity environment, Sol. Energy **219**, 50 (2021). https://doi.org/10.1016/j.solener.2020.10.022
17. G. Chowdhury, M. Haggag, J. Poortmans, How cool is floating PV? A state-of-the-art review of floating PV's potential gain and computational fluid dynamics modeling to find its root cause, EPJ Photovolt. **14**, 24 (2023). https://doi.org/10.1051/epjpv/2023015
18. S. Kaplanis, E. Kaplani, J.K. Kaldellis, PV temperature prediction incorporating the effect of humidity and cooling due to seawater flow and evaporation on modules simulating floating PV conditions, Energies **16**, 12 (2023). https://doi.org/10.3390/en16124756
19. M. Almaktar, H.A. Rahman, M.Y. Hassan, S. Rahman, Climate-based empirical model for PV module temperature estimation in tropical environment, Appl. Sol. Energy **49**, 192 (2013). https://doi.org/10.3103/S0003701X13040026
20. E. Barykina, A. Hammer, Modeling of photovoltaic module temperature using Faiman model: sensitivity analysis for different climates, Sol. Energy **146**, 401 (2017). https://doi.org/10.1016/j.solener.2017.03.002
21. D. Faiman, Assessing the outdoor operating temperature of photovoltaic modules, Prog. Photovolt.: Res. Appl. **16**, 307 (2008). https://doi.org/10.1002/pip.813
22. S. Mathew, *Wind Energy: Fundamentals, Resource Analysis and Economics* (Springer, Berlin/Heidelberg, 2006)
23. D. Lindholm, J. Selj, T. Kjeldstad, H. Fjær, V. Nysted, CFD modelling to derive *U*-values for floating PV technologies with large water footprint, Sol. Energy **238**, 238 (2022). https://doi.org/10.1016/j.solener.2022.04.028
24. W.C.L. Kamuyu, J.R. Lim, C.S. Won, H.K. Ahn, Prediction model of photovoltaic module temperature for power performance of floating PVs, Energies **11**, 447 (2018). https://doi.org/10.3390/en11020447
25. G.M. Tina, F. Bontempo Scavo, L. Merlo, F. Bizzarri, Comparative analysis of monofacial and bifacial photovoltaic modules for floating power plants, Appl. Energy **281**, 116084 (2021). https://doi.org/10.1016/j.apenergy.2020.116084
26. A. Vasel, F. Iakovidis, The effect of wind direction on the performance of solar PV plants, Energy Convers. Manag. **153**, 455 (2017). https://doi.org/10.1016/j.enconman.2017.09.077
27. D. Waterworth, A. Armstrong, Southerly winds increase the electricity generated by solar photovoltaic systems, Sol. Energy **202**, 123 (2020). https://doi.org/10.1016/j.solener.2020.03.085
28. E. Kaplani, S. Kaplanis, Thermal modelling and experimental assessment of the dependence of PV module temperature on wind velocity and direction, module orientation and inclination, Sol. Energy **107**, 443 (2014). https://doi.org/10.1016/j.solener.2014.05.037
29. N.A.S. Elminshawy, A. Osama, D.G. El-Damhogi, E. Oterkus, A.M.I. Mohamed, Simulation and experimental performance analysis of partially floating PV system in windy conditions, Sol. Energy **230**, 1106 (2021). https://doi.org/10.1016/j.solener.2021.11.020
30. T. Kjeldstad, V.S. Nysted, M. Kumar, S. Oliveira-Pinto, G. Otnes, D. Lindholm, J. Selj, The performance and amphibious operation potential of a new floating photovoltaic technology, Sol. Energy **239**, 242 (2022). https://doi.org/10.1016/j.solener.2022.04.065
31. PVsyst, Project design > Array and system losses > Array Thermal losses, accessed: Feb. 7, 2024. https://www.pvsyst.com/help/thermal_loss.htm
32. D. Shankar, P.N. Vinayachandran, A.S. Unnikrishnan, The monsoon currents in the north Indian Ocean, Prog. Oceanogr. **52**, 63 (2002). https://doi.org/https://doi.org/10.1016/S0079-6611(02)00024-1
33. D.L. King, W.E. Boyson, J.A. Kratochvill, Photovoltaic Array Performance Model (2004)
34. D.C. Wilcox, *Turbulence Modeling for CFD* (DCW Industries, 2006)
35. S. Rodriguez, *Applied Computational Fluid Dynamics and Turbulence Modeling* (Springer Verlag, 2019). https://doi.org/10.1007/978-3-030-28691-0
36. W.C. Swinbank, Long-wave radiation from clear skies, Q. J. R. Meteorol. Soc. **89**, 339 (1963). https://doi.org/10.1002/qj.49708938105
37. IEC, IEC 61853 Photovoltaic (PV) module performance testing and energy rating – Part 2: Spectral responsivity, incidence angle and module operating temperature measurements (2016)
38. H. Goverde, D. Goossens, J. Govaerts, V. Dubey, F. Catthoor, K. Baert, J. Poortmans, J. Driesen, Spatial and temporal analysis of wind effects on PV module temperature and performance, Sustain. Energy Technol. Assess. **11**, 36 (2015). https://doi.org/10.1016/j.seta.2015.05.003.

Cite this article as: Vilde Stueland Nysted, Dag Lindholm, Josefine Selj, Torunn Kjeldstad, Floating photovoltaics: modelled and experimental operating temperatures and the impact of wind speed and direction, EPJ Photovoltaics **15**, 23 (2024)